COMPLEX NETWORK FOR SOLAR ACTIVE REGIONS

FARHAD DAEI, ¹ HOSSEIN SAFARI, ¹ AND NEDA DADASHI ¹

¹Department of Physics, Faculty of Science, University of Zanjan, P. O. Box 45195-313, Zanjan, Iran

(Received November 16, 2018; Revised; Accepted)

Submitted to ApJ

ABSTRACT

Here, we developed a complex network of solar active regions (ARs) to study various local and global properties of the network. The values of the Hurst exponent (0.8-0.9) were evaluated by both the detrended fluctuation analysis and the rescaled range analysis applied on the time series of the AR numbers. The findings suggest that ARs can be considered as a system of self-organized criticality. We constructed a growing network based on locations, occurrence times, and the lifetimes of 4,227 ARs recorded from 1 January 1999 to 14 April 2017. The behaviour of the clustering coefficient shows that the ARs network is not a random network. The logarithmic behaviour of the length scale has the characteristics of a so-called "small-world network". It is found that the probability distribution of the node degrees for undirected networks follows the power-law with exponents of about 3.7 to 4.2. This indicates the scale-free nature of the ARs network. The scale-free and small-world properties of the ARs network confirm that the system of ARs forms a system of self-organized criticality. Our results show that the occurrence probability of flares (classified by GOES class C > 5, M, and X flares) in the position of the ARs network hubs take values greater than that obtained for other nodes.

Corresponding author: Hossein Safari

safari@znu.ac.ir

Keywords: Sun: Active Regions, Sun: Flares, Sun: Activity

1. INTRODUCTION

Solar active regions (ARs) are the origin of various energetic phenomena. It is believed that solar flares and coronal mass ejections are direct results of the changes in the topology and structure of the ARs' magnetic field (Priest & Forbes 2002; Aschwanden 2005). Because of the important role of ARs in solar activity, numerous attempts have been made to study the statistical properties of ARs (Künzel 1959; Howard 1989, 2000; Sammis et al. 2000; Leka & Barnes 2003; Georgoulis & Rust 2007; Schrijver 2007; Falconer et al. 2008; Mason & Hoeksema 2010; Falconer et al. 2011; Georgoulis et al. 2012; Abramenko 2015; Arish et al. 2016; Barnes et al. 2016; Raboonik et al. 2017). Zhang et al. (2010) studied both the statistical (e.g. the frequency distribution of size and magnetic flux) and physical properties of 1,730 ARs detected from 1996 to 2008. The information (occurrence times and locations on solar disk) about ARs and sunspots are recorded by the Royal Observatory of Belgium (ROB), the Solar Influences Data Analysis Center (SIDC), and the National Oceanic and Atmospheric Administration (NOAA). In the NOAA catalog, each AR has a unique identification number. There is important evidence to suggest that systems of solar events such as flares, bright points, and so on are in a self-organized criticality (SOC) (Zhang et al. 2001; Alipour & Safari 2015; Aschwanden et al. 2016). Aschwanden (2013) provided an extended review on SOC in solar physics and astrophysics. de Arcangelis et al. (2006) studied the universality properties of both solar flares and earthquakes. They showed that both phenomena follow the same law for the size distribution and inter-occurrence times. Also, they interpreted the temporal power-law dependency of the afterflare sequence as the Omori law for earthquakes.

The complex network is an approach to study effectively large complex systems (e.g. earthquakes, bulk electrical power systems, computers, the brain, and social systems). This approach explains significant characteristics of complex systems using network representations that have their roots in mathematical studies and are known as the graph theory. In most studies, a network or its equivalent graph is considered as a collection of some nodes together with edges while modeling a network (Newman 2003; Humphries & Gurney 2008; Rubinov & Sporns 2010; Lotfi & Darooneh 2012, 2013; Rezaei et al. 2017). Probability theory is a useful tool for interpreting the details of

small-world networks.

the complexity of the networks. The scale-free and small-world networks are the two main complex networks that have been widely used to study large complex systems (e.q. Watts & Strogatz 1998; Amaral et al. 2000; Barabási & Bonabeau 2003; Kim & Wilhelm 2008; Buldyrev et al. 2010). Smallworld networks are basically intersections of the random and regular networks. In these kinds of networks, the length scale behaviour is the same as in the random networks, but with a high average in the clustering coefficient (Watts & Strogatz 1998). The quantitative measurement of the small-world property can be computed by different methods-all comparing the network's parameters with the parameters of an equivalent random or regular network (Humphries & Gurney 2008; Telesford et al. 2011). Humphries & Gurney (2008) presented a measure for the small-world property of a network by comparing both its length scale and clustering coefficient with an equivalent random network. This factor is employed in many articles, especially in the field of neuroscience (Bullmore & Sporns 2009). However, Telesford et al. (2011) explained that the Humphries method cannot correctly recognize the small-world networks. They introduced a new factor, using the length scale of a random network and the clustering coefficient of a regular network to evaluate the small-world property of a network. In this paper, we construct a network for the ARs using their locations, occurrence times, and lifetimes. We compute the length scale, clustering coefficient, and degree distribution of nodes for the network. We describe important properties of the ARs network in the category of scale-free and

The details are discussed as follows: Section 2 introduces the data set. In Section 3, the application of both detrended fluctuation and rescaled range (R/S) analysis on the time series of ARs is explained. Sections 4 and 5 describe the construction of ARs networks and their properties. Sections 6 and 7 present the results and conclusions, respectively.

2. DATA PROCESSING

The solar monitor (www.solarmonitor.org) records the solar data observed by several solar space observatories and missions (e.g. GOES, GONG, ACE, STEREO, SDO, etc.).

SolarMonitor.org provides daily tables for ARs that occur on the main-side of the sun. The daily tables include the unique identification NOAA numbers, sunspot areas, Hale and McIntosh classi-

fications, produced flares, and the number of spots (Gallagher et al. 2002). The AR positions are tabulated daily in both the heliographic (in latitude and longitude) and heliocentric (in arcsec) coordinates. The needed information of 4,227 ARs during 1 January 1999 to 14 April 2017 for building the ARs network are the NOAA numbers, rotated positions, occurrence times, and lifetimes. By tracking the NOAA numbers in daily tables, the lifetimes and positions of the ARs are extracted. The appendix of this paper contains a table that includes the NOAA numbers, dates, and positions in the heliographic coordinates (longitudes and latitudes) for 4,227 ARs. Using the diff_rot code in the SunPy software (SunPy Community et al. 2015), the locations of the ARs are rotated with respect to the first occurrence time of the reference AR (NOAA 8419). For more simplicity, we used the location of the ARs at their first occurrence time during their lifetimes (on the main-side). In Figure 1, the rotated positions at the first occurrence time of 4,227 ARs in the front and far hemispheres are presented. The rotated positions of ARs (longitudes (φ) and latitudes (θ)) are restricted to the range of $0^{\circ} - 360^{\circ}$ and $0^{\circ} - 180^{\circ}$, respectively.

Using the GOES flare catalog (ftp://ftp.ngdc.noaa.gov/STP/space-weather/solar-data/solar-featu we identify ARs including energetic flares (C>5, M, and X class) during 1 January 1999 to 14 April 2017.

3. HURST EXPONENT

The Hurst exponent is a key parameter to measure the auto correlation (self-dependency) of the time series. Both the detrended fluctuation analysis (DFA) (Mandelbrot 1975; Peng et al. 1994; Weron 2002; Alipour & Safari 2015) and R/S analysis (Buldyrev et al. 1995; Weron 2011) are useful tools to study the self-affinity (temporal dependency) in the time series of ARs (Figure 2). In order to compute the Hurst exponent, the time series of ARs x(t) with length T is divided into adjacent subtime series of length P while T=mP. Each sub-time series is labeled by $x_i^j(t_i)$ (i = 1, ..., P, j = 1, ..., m). For each sub-time series, the rescaled range (R/S) is computed by

$$(R/S)_{j} = \frac{\max(y_{1}^{j}, ..., y_{P}^{j}) - \min(y_{1}^{j}, ..., y_{P}^{j})}{\sqrt{\frac{1}{P-1} \sum_{i=1}^{P} (x_{i}^{j} - \bar{x}^{j})}},$$
(1)

where $\bar{x}^j = \frac{1}{P} \sum_{i=1}^P x_i^j$ and $y_k^j = \sum_{i=1}^k (x_i^j - \bar{x}^j), k = 1, ..., P$. The average of the normalized range for the P sub-time series is given by $(R/S)_P = \frac{1}{m} \sum_{j=1}^m (R/S)_j$. Mandelbrot (1975) and Weron (2002) have shown that the R/S analysis shows asymptotic behaviour as $(R/S)_P \propto P^H$, in which H is the Hurst exponent, which can be obtained from a linear fit in the log-log scale of $(R/S)_P$ versus P.

In the DFA for each cumulative time series $\sum_{i=1}^{k} (x_i^j - \bar{x}^j)$, a straight line $\alpha_j t_i + \beta_j$ is fitted. The mean value of the mean square fluctuation for all sub-time series is computed using

$$F(P) = \frac{1}{m} \sum_{j=1}^{m} \left(\frac{1}{P} \sum_{i=1}^{P} ((x_i^j - \bar{x}^j) - \alpha_j t_i - \beta_j)^2 \right)^{1/2}.$$
 (2)

The Hurst exponent (H) can be obtained by a linear fit (in a log-log scale) for F(P) versus P.

DFA and R/S analyses are used to extract the value of the Hurst exponent (H) to investigate the behaviour of the time series. In the analysis of time series based on the value of the Hurst exponent (H), if 0 < H < 0.5 and 0.5 < H < 1, we can say the time series has long temporal negative and positive correlations, respectively. If H equals to 0.5, the time series is uncorrelated (white noise) (Buldyrev et al. 1995). By applying the DFA and R/S on the time series of ARs, the values of the Hurst exponent are obtained as 0.8 and 0.94, respectively. These values show that the time series of ARs has a long temporal dependency and suggest that the system of ARs is one of SOC (Carreras et al. 2001; Dobson et al. 2007; Alipour & Safari 2015). SOC is an important way to describe the complex nature of a high degree of freedom and non-linearity in many physical and astrophysical phenomena (e.g. Bak et al. 1987; Tang & Bak 1988; Wang & Dai 2013; Aschwanden et al. 2016)

In the remainder of this paper, we study the behaviour of the SOC of the ARs system in the framework of the complex network.

4. ACTIVE REGIONS NETWORK

The information of 4,227 recorded ARs is used to construct a complex network concerning the following steps:

- The solar spherical surface is divided into $N \times N$ cells with equal areas considering the spherical coordinates (θ, φ) as $A_{i,j} = \frac{4\pi}{N^2} R_{\odot}^2$, i, j = 1..N, where the parameter R_{\odot} is the solar radius.

The angles θ and φ for each equal area cell are given by:

$$\varphi_{i+1} = \varphi_i + \frac{2\pi}{N} , \ \varphi_1 = 0,$$

$$\cos(\theta_{j+1}) = \cos(\theta_j) - \frac{1}{N} , \ \theta_1 = 0.$$
(3)

- The ARs are assigned to cells according to their locations at their first occurrence times rotated with respect to the first occurrence time of the reference AR (NOAA 8419) (Figure 1). To avoid more complexity in our analysis, the variations on the latitudes and longitudes of ARs during their lifetimes are ignored. Cells with no ARs are removed from our network analysis. However, the remaining ones are used as the nodes of the network, indicated by n_{ℓ} ($\ell = 1..L$).
- An edge connects the node n_i to n_j if an AR appears at node (cell) n_j during the lifetime of another AR at node n_i . A loop (connecting node n_i to itself) is formed when an AR appears during the lifetime of another one within the same cell. In Figure 3, a small part of the ARs network with six nodes, 15 edges, and four loops is shown. This graph presents a sample of our network, which contains the information of 33 ARs. The AR NOAA 10081 is formed during the lifetime of AR NOAA 10063; therefore, in our network, the node number 680 is connected to the node that is labeled by 557. Also, the AR NOAA 9805 appeared in the lifetime of AR NOAA 9794 at the same node (681); so, a loop is created.
- We organize a directed and weighted network as an $L \times L$ adjacency matrix (A'). In order to analyze the properties of the ARs network, A' is converted to a symmetric matrix with all diagonal elements equal to zero, which is representative of the undirected, unweighted, and self-loop-free graph.

5. NETWORK PARAMETERS

A graph that consists of nodes and edges is a mathematical representation of a network. In general, a graph can be categorized into a directed or an undirected and a weighted or an unweighted graph depending on its edges. A directed network or its equivalent graph is defined by a set of nodes including directed connections (edges). A graph with bi-directional edges is called an undirected

graph. A graph with different real numbers assigned to its edges is named a weighted network. The unweighted ones are those for which all the weights are set to be equal to one or the edges have no number assigned to them. In the complex network approach, using the adjacency matrix made for a graph, the topological properties in both the local and global scales were studied (Steen 2010). In the present section, we briefly review some network parameters.

In order to characterize a graph, one can use an adjacency matrix (A'), including information about edges and nodes. The adjacency matrix is an $L \times L$ matrix in which the element $a'_{i,j}$ is the number of edges (i.e. weight of edge) connecting node n_i to node n_j . In this way, the sum of i^{th} row elements represents the outbound edges from the node n_i (outbound degree) and the sum of the i^{th} column elements represents the number of inbound edges to the node (inbound degree). The diagonal elements represent self-loop(s) of nodes (i.e. a node connecting to itself by an edge). For a simple undirected and unweighted graph, the adjacency matrix is a symmetric matrix with all elements equal to zero or one. Undirected and unweighted adjacency matrices are used to determine the characteristics of the ARs network, including the average of local clustering coefficients, mean of shortest path length, diameter, and the nodes' degree of probability distribution function.

To convert the network to an unweighted, undirected, and loop-free network, the diagonal elements of the adjacency matrix are set to zero and every non-zero element is replaced by one. Then, the new adjacency matrix (A) is symmetrized.

The local clustering coefficients (c_i) and clustering coefficient (C) are computed using the adjacency matrix A:

$$c_i = \frac{\sum_{j,\ell \neq i} a_{i,j} a_{j,\ell} a_{\ell,i}}{k_i (k_i - 1)},\tag{4}$$

$$C = \frac{1}{L} \sum_{i=1}^{L} c_i, \tag{5}$$

where k_i and L are the number of edges connected to the i^{th} node and the total number of nodes, respectively.

The average of the shortest path between all pairs of nodes is another interesting parameter of the network, expressed as:

$$ls = \frac{1}{L(L-1)} \sum_{i,j=1, i \neq j}^{L} d_{i,j}, \tag{6}$$

where $d_{i,j}$ is the shortest path length between i and j nodes.

The parameter $d_{i,j}$ is computed using Floyd-Warshall algorithm (Floyd 1962), which is an efficient method to find the length of the shortest path between all nodes in a graph. The largest value of the shortest paths is called the diameter of a graph. Another interesting property of a network is the probability distribution function (PDF) of the nodes' degree, which determines the probability of finding a node with a certain degree.

In this study, we refer to some properties of such well-known networks as regular, random, small-world, and scale-free networks.

In regular graphs with all nodes having the same degree, typically the clustering coefficient and shortest path length possess large values. A network is called random if all pairs of nodes are connected with the same probability (Erdos & Rényi 1960). A random graph, in comparison with a regular one, has smaller values for both the clustering coefficient and the shortest path length. For a random network, the average values of the shortest path length (ls_{rand}) and clustering coefficient (C_{rand}) can be obtained by the following equations:

$$ls_{\rm rand} = \frac{\ln(L_{\rm rand}) - \gamma}{\ln \langle k \rangle} + \frac{1}{2},\tag{7}$$

$$C_{\rm rand} \simeq \frac{E_{\rm rand}}{L_{\rm rand}^2},$$
 (8)

where $E_{\rm rand}$, $L_{\rm rand}$, < k >, and $\gamma = 0.5772$ are the number of nodes, number of edges, average degree of nodes, and Euler constant, respectively (Fronczak et al. 2004). One can build a random graph using a model proposed by Erdos & Rényi (1960). The intersection of the random and regular graphs is called a small-world graph (Watts & Strogatz 1998). A small-world graph has a small average shortest path. However, the clustering coefficient takes the larger value. We can find enough examples of such graphs in nature—for instance, in the brainstem reticular network (Humphries et al. 2005), human

protein network (Stelzl et al. 2005), and power grid network (Mei et al. 2011). Bullmore & Sporns (2009) reviewed the small-world networks in neurosciences. In some small-world networks (e.g. the brainstem reticular network), the PDF of the nodes' degree (P(k)) follows a power-law, $P(k) \propto k^{-\gamma}$. This kind of network is representative of scale-free events.

6. RESULTS

In order to construct a complex network for the solar ARs, the locations and dates of the first occurrence times, and the lifetimes of 4,227 ARs were used (Section 4). The nodes of network was created by dividing the solar surface into equal area cells. The adjacency matrix was prepared for both the directed and undirected ARs networks. The weighted adjacency matrix was determined using directed connections (edges) between the pair of ARs. Loops, the connections between two successive ARs occurring at the same cell (node), were considered as the diagonal elements of the adjacency matrix $(a'_{i,i})$. The empty cells of the directed and weighted adjacency matrix were removed from our network analysis. The effect of the network size (the number of nodes, L) on the shortest path length, clustering coefficient, and probability distribution of the nodes' degree are studied. An equivalent random network was constructed corresponding to the ARs network with the same size and edges.

The clustering coefficients of the ARs networks and their equivalent random networks (with the same number of nodes and edges) are shown in Figure 4. The size of the networks varies from 54 to 2,693 (nodes). The clustering coefficient for the ARs and random networks are computed by Eqs. (4) and (7), respectively. It is found that the clustering coefficient of the ARs network is noticeably greater than the equivalent random network by about a factor of two or more.

In Figure 5, the length scale of the ARs network versus the size (logarithm) of the network is plotted. For small size of the ARs networks (L < 500) most of the nodes are connected together and the networks tend to the complete graphs. For the networks with size 500-2,700 a linear fitting was applied and the slope of the fit was obtained ($ls = 0.79 \log_{10} L$). According to the small values of the length scale and its logarithmic dependency on the size, we conclude that the ARs network is classified as a small-world network.

Figure 6 presents the PDF of the nodes' degree for the undirected networks with the size varying from 1,687 to 2,693. The lower ends of the degree distributions ($k < k_{trunc}$) suffer from some truncation effects due to incomplete detection of small ARs and far-side ARs, therefore should not be considered in the power-law fitting. The truncated power-law ($p(k) \sim k^{-\gamma}$) fitting was carried out on the probability distribution of the nodes' degree (Aschwanden 2015). The values of the power-law exponent range from 3.7 to 4.2. The power-law nature of the PDF indicates that a few nodes have high connectivity values. In the context of the complex network, nodes with a large number of connections are named hubs of the network (Albert & Barabási 2002). One may ask: What is the criterion for selecting a node as a hub? In a network, nodes with degrees higher than a threshold are considered as hubs. The threshold is defined as the maximum degree of nodes in the equivalent random network.

We found that for the ARs network with 1,986 nodes, there are 53 hubs with degrees larger than 80. On increasing the network size to 2,693 nodes, 78 hubs with connections larger than 61 are found. In Figure 7, the relation between the average number of large energetic flares (C> 5, M, and X classes) appearing at the position of the ARs network nodes is presented. The average number of flares increases with an increase in the degree of the nodes. The average number of large flares appearing at the position of the ARs network hubs is larger than the other nodes by at least a factor of two. In Figure 8, the dependency of the averaged local clustering coefficient (\bar{C}) for the nodes with the same degree is presented. The threshold power-law($\bar{C} \sim (k + k_{\rm th})^{-\gamma}$) is fitted to the average local clustering coefficient in which $k_{\rm th}$ is the threshold value. Aschwanden (2015) modeled the threshold power-law for size distributions of some natural phenomena (e.g., solar and stellar flares, etc.). They show that in most size distributions of detected data, the threshold power-laws are significantly well fitted. We found that by increasing the size of the network, the power-law exponent of the average clustering coefficient slightly exceeds the value one.

7. CONCLUSION

Typically, 220 ARs can be observed on the solar disk each year. Within some of the ARs, large-scale magnetic phenomena such as flares and coronal mass ejections are stochastically emerged. The exact

physical mechanism underlying these phenomena remains unknown. The results of applying both the detrended fluctuation and R/S analysis with the Hurst exponent (0.8 - 0.9) suggest that the ARs system is categorized into SOC, which motivated us to confirm such a characteristic by using the complex network approach. In the present work, we designed the ARs network based on their locations at the first occurrence times and lifetimes. In our complex network, all ARs that occurred in the lifetime of a specific AR are linked with each other. The unweighted adjacency matrix was used to calculate the length scale and clustering coefficient of the network. The degree of nodes was computed for both the directed and undirected ARs networks. The main results of this study are organized as follows:

- A comparison between both the values and behaviour of the clustering coefficient of the ARs network and the equivalent random network (with the same number of edges and nodes) indicates that the ARs network is not a random network.
- The small values of the length scale and its logarithmic behaviour ($ls = 0.74 \log_{10} L$) related to the network size demonstrate that the ARs network is a small-world network. The obtained results for the large values of the clustering coefficient confirm that the ARs network can be classified in a category of the small-world network.
- The truncated power-law distribution was fitted to the PDF of the nodes' degree. The power-law nature of the nodes' degree demonstrates the scale-free feature of the ARs network. Recent observations have shown that some of the ARs produce energetic phenomena (e.g. flares, CMEs, etc) and some others do not. Such characteristics of the ARs network are representative of the prescription of the heterogeneous networks (e.g. Abe & Suzuki 2009).
- We observed an increase in flare occurrence in each cell corresponding to the hubs. In other words, the nodes with higher degrees in the ARs network have a higher likelihood to trigger flares (Figure 7). This behaviour of the ARs network raises an important question about the prediction capability of flares based on the ARs network. More statistical studies are required to examine the flare prediction with the ARs' complex network.

In the present study, we used the ARs information appearing on the main-side of the solar surface. By employing the tracking algorithms on the reconstructed helioseismic maps (Lindsey & Braun 2000; Hernndez et al. 2013), the returning far-side ARs can be identified. By increasing the lifetimes of some ARs from two weeks to one month or more, the number of connections (edges and loops) for some nodes of the ARs network may be increased. Additionally, some of the nodes may be empty and, therefore, will be removed from the analysis. Expectedly, by decreasing the number of nodes in the presence of the ARs with the large lifetimes, the diameter and the mean path length of the network may also decrease while the clustering coefficient may increase. More quantitative studies are required to address the effects of the far-side ARs information on the properties of the network. In the next step, we attempt to include more characteristics of ARs (e.g. magnetic class, Hall class, McIntosh class, sunspots) and study the effects of changing solar latitudinal and longitudinal displacements of the ARs during their lifetimes in order to investigate the prediction capability for energetic solar events.

ACKNOWLEDGEMENT

The authors thank the unknown referee for his/her very helpful comments and suggestions. Data supplied courtesy of SolarMonitor.org.

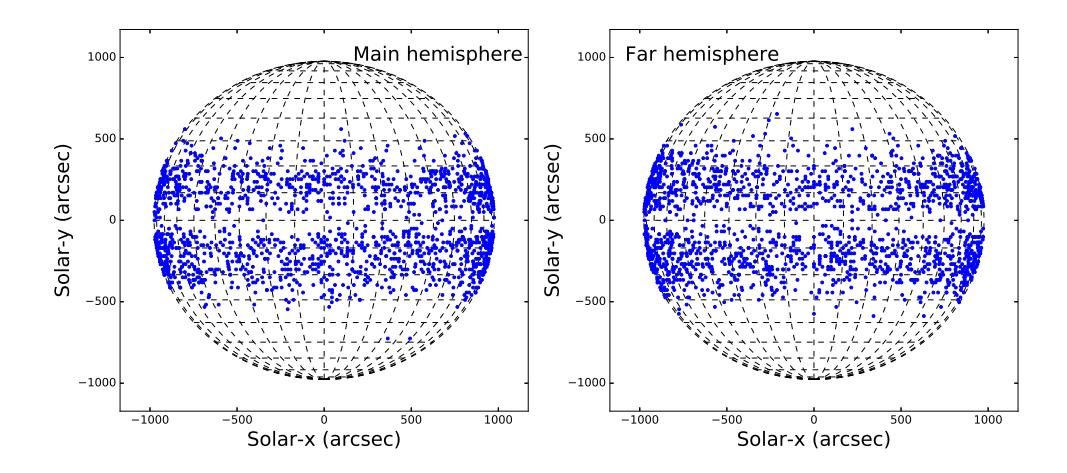


Figure 1. Positions of 4,227 ARs (from 1 January 1999 to 14 April 2017) at their first occurrence times, rotated with respect to the first AR (NOAA 8419) coordinates. All positions longitudes and latitudes are restricted to $0^{\circ} - 360^{\circ}$ and $0^{\circ} - 180^{\circ}$, respectively, and are mapped to the surface of a sphere (see text).

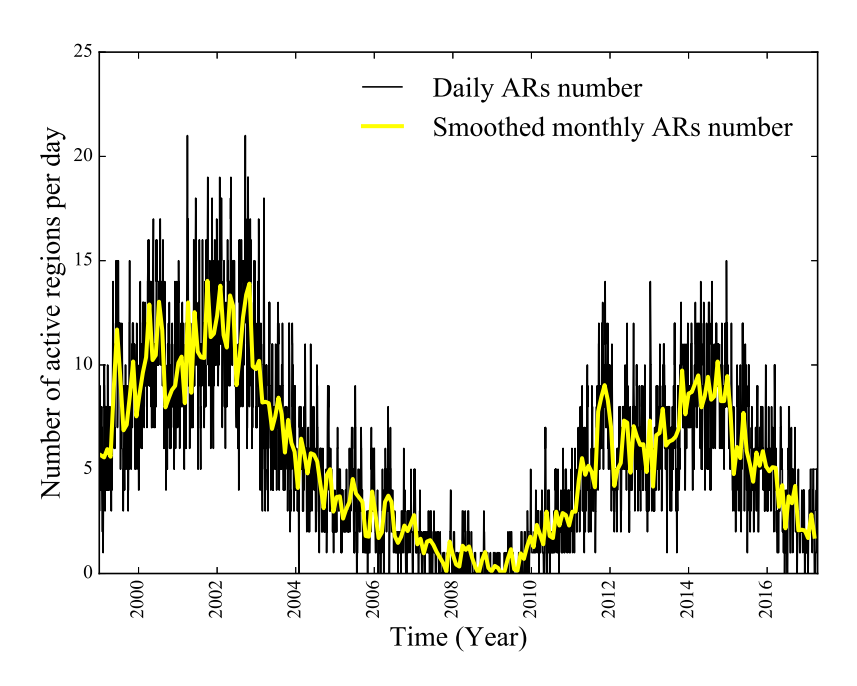


Figure 2. Time series of ARs daily (black line) and smoothed monthly (yellow line) from 1 January 1999 to 14 April 2017 on the solar main-side, which includes 4,227 ARs.

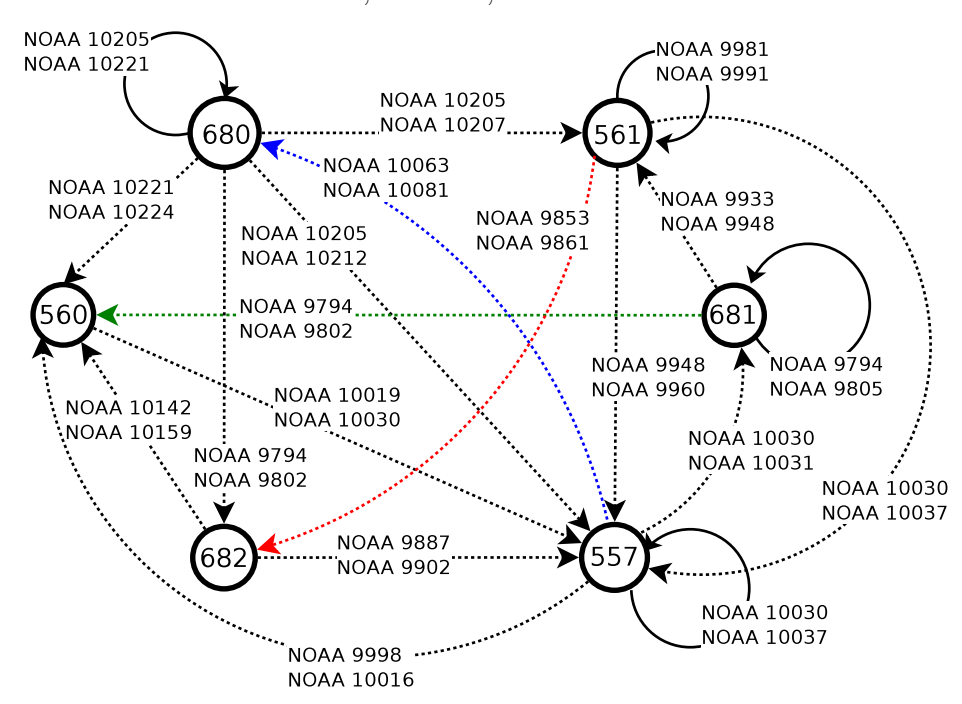


Figure 3. A small part of the ARs network comprising six nodes is represented. Each arrow represents the edge between the two nodes. For example, the AR (NOAA 10081) emerges in node n_{680} during the lifetime of AR (NOAA 10063) presented in node n_{557} , so that a directed edge is drawn from n_{557} to n_{680} . Each self-loop shows the occurrence of two coinciding ARs in the same node. For example, the AR (NOAA 10205) appearing at the same node of AR (NOAA 10221) formed the self-loop.

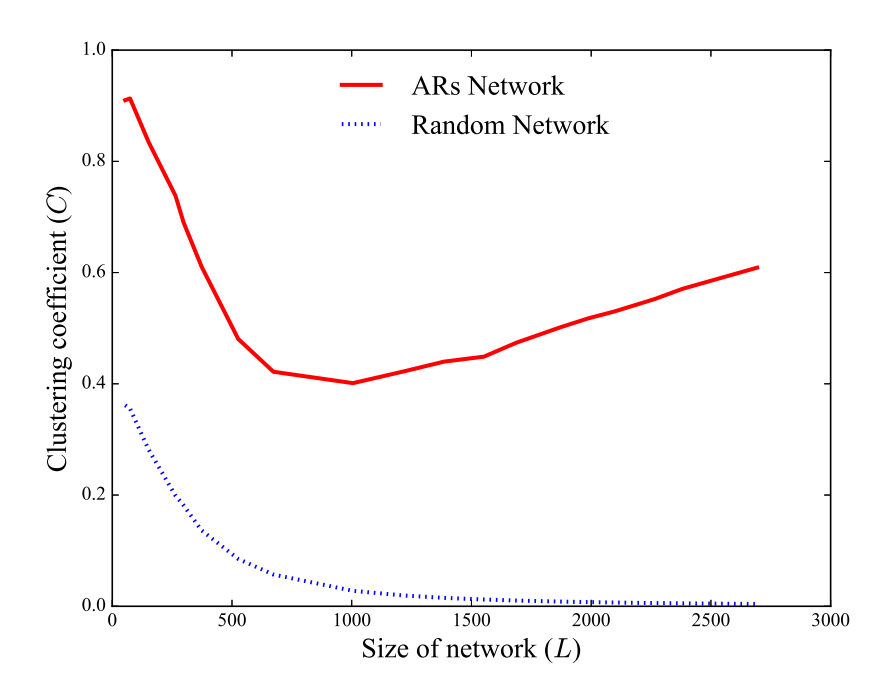


Figure 4. Clustering coefficient of ARs networks and their equivalent random networks (with the same number of nodes and edges) are plotted. The size of the network ranges from 50 to 2,700 (nodes).

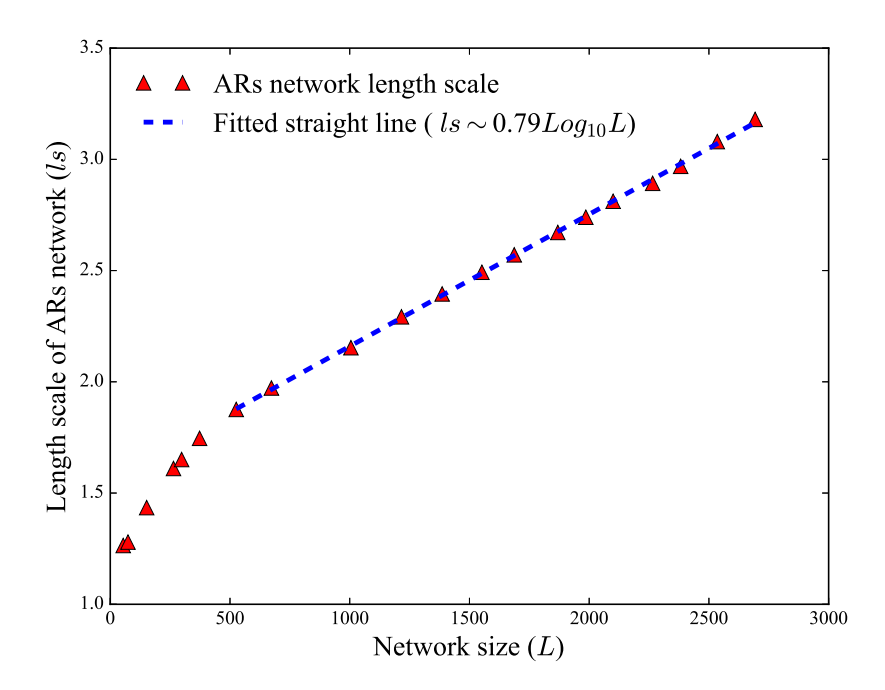


Figure 5. Length scale of the ARs network (triangle) versus the network size (L) and a fitted straight line as $ls \sim 0.79 \, \log_{10} L$ are plotted.

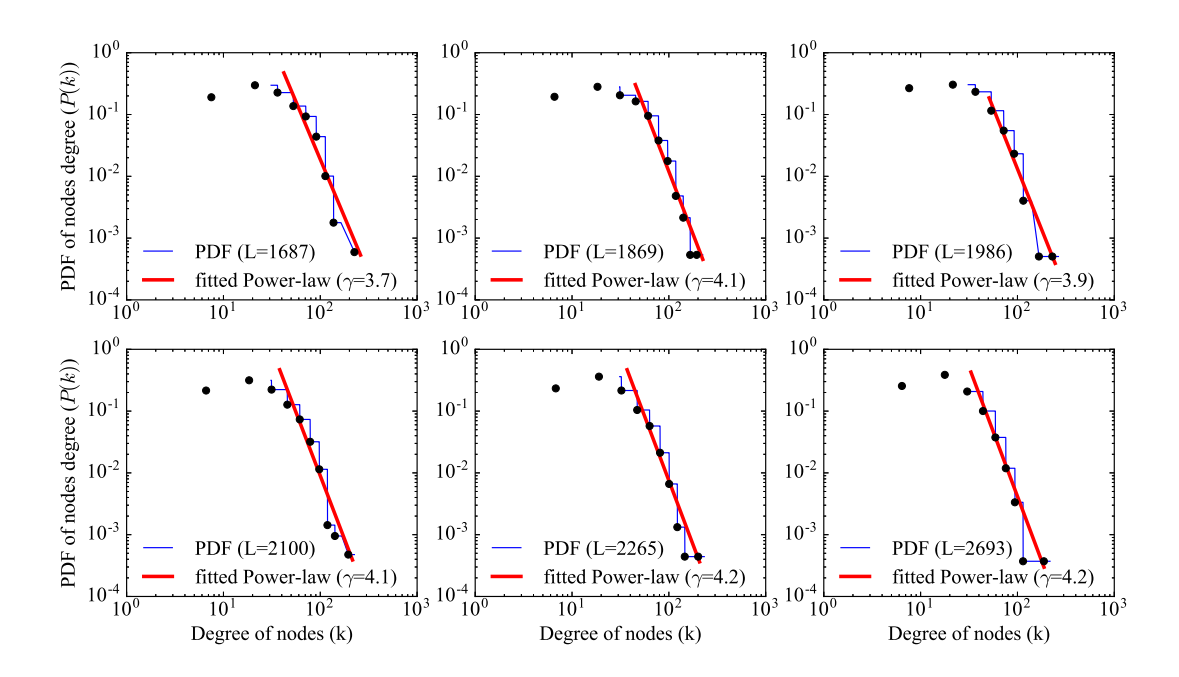


Figure 6. Probability distribution function (PDF) for the nodes' degrees (circles) for undirected ARs network are plotted in a log-log scale. The exponent for the fitted truncated power-laws (dashed line) is obtained in the range of 3.7-4.2.

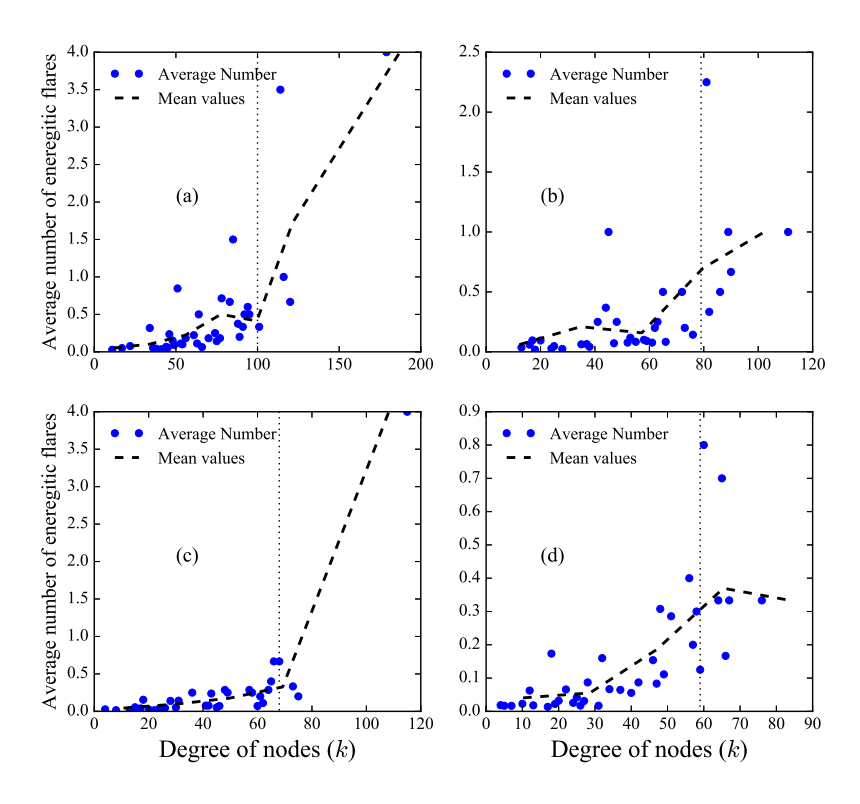


Figure 7. The average number of flares (circles) and connected mean values of non-uniform binning (dashed line) observed within the position of the ARs network nodes versus the degree of nodes for the network size (L) (a) 1,552, (b) 1,986, (c) 2,382, and (d) 2,693 are plotted. The nodes with high degrees (hubs) are presented on the right side of the dotted lines.

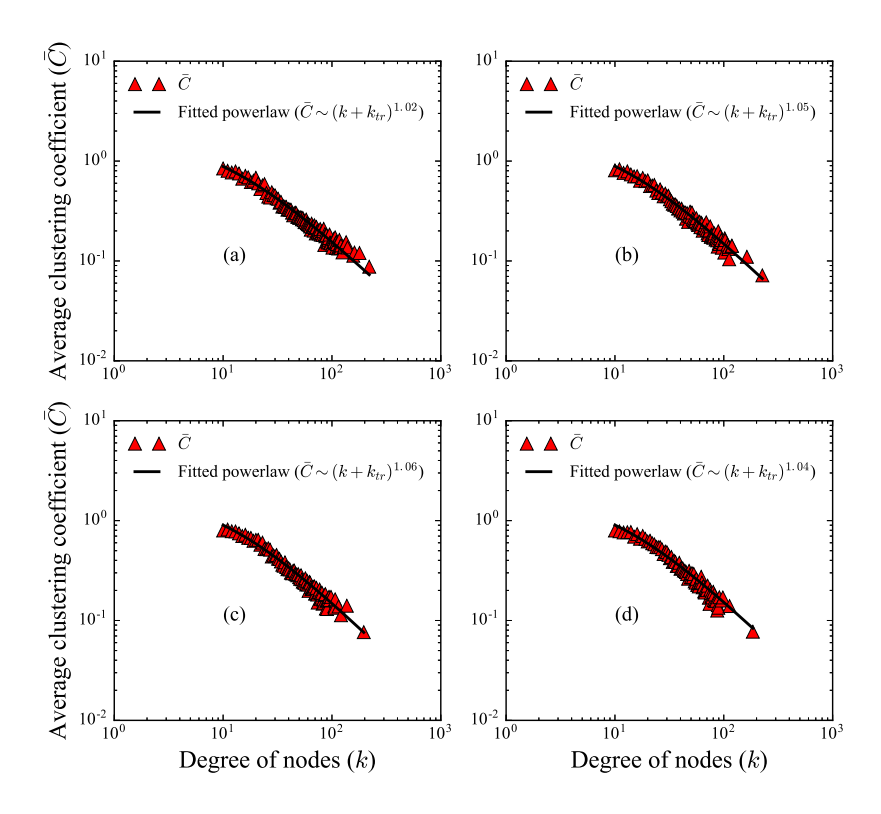


Figure 8. The average of the clustering coefficients of nodes with the same degree (triangles) in the undirected ARs networks and the fitted threshold power-laws ($C \sim (k + k_{th})^{-\gamma}$) are presented for network sizes (a) 1,552, (b) 1,986, (c) 2,382, and (d) 2,693. The value of the threshold (k_{th}) selected to be 10 and the fitted power-law exponents obtained to be in the range of 1.02 – 1.06.

Table 1. Solar Active Regions data

ID	Year	Month	Day	Lat.	Long.
8419	1999	01	01	28	91
8419	1999	01	02	28	77
8420	1999	01	01	20	43
8420	1999	01	02	20	40
8420	1999	01	03	20	39
8421	1999	01	01	27	40

NOTE—Table 1 is published in its entirety in the electronic edition of the *Astrophysical Journal*. A portion is shown here for guidance regarding its form and content.

APPENDIX

REFERENCES

Abe, S., & Suzuki, N. 2009, Brazilian Journal of Physics, 39, 428

Abramenko, V. I. 2015, Geomagnetism and Aeronomy, 55, 860

Albert, R., & Barabási, A.-L. 2002, Rev. Mod. Phys., 74, 47

Alipour, N., & Safari, H. 2015, The Astrophysical Journal, 807, 175

Amaral, L. A., Scala, A., Barthelemy, M., & Stanley, H. E. 2000, Proc. Natl. Acad. Sci. U. S. A., 97, 11149 Arish, S., Javaherian, M., Safari, H., & Amiri, A. 2016, Solar Physics, 291, 1209

Aschwanden, M. 2005, Physics of the Solar Corona, 1st edn. (Springer-Verlag Berlin Heidelberg), doi:10.1007/3-540-30766-4

Aschwanden, M. J. 2013, Self-Organized Criticality Systems (Open Academic Press)

Aschwanden, M. J. 2015, The Astrophysical Journal, 814, 19

Aschwanden, M. J., Crosby, N. B., Dimitropoulou, M., et al. 2016, Space Science Reviews, 198, 47

- Bak, P., Tang, C., & Wiesenfeld, K. 1987, Phys.Rev. Lett., 59, 381
- Barabási, A.-L., & Bonabeau, E. 2003, Scientific American, 50
- Barnes, G., Leka, K. D., Schrijver, C. J., et al. 2016, ApJ, 829, 89
- Buldyrev, S. V., Goldberger, A. L., Havlin, S., et al. 1995, Phys. Rev. E, 51, 5084
- Buldyrev, S. V., Parshani, R., Paul, G., Stanley, H. E., & Havlin, S. 2010, Nature, 464, 1025
- Bullmore, E., & Sporns, O. 2009, Nat. Publ. Gr., 10, 186
- Carreras, B. A., Newman, D. E., Dobson, I., & Poole, A. B. 2001, in Proceedings of the 34th Annual Hawaii International Conference on System Sciences, 705–709
- de Arcangelis, L., Godano, C., Lippiello, E., & Nicodemi, M. 2006, Phys. Rev. Lett., 96, 051102
- Dobson, I., Carreras, B. A., Lynch, V. E., & Newman, D. E. 2007, Chaos: An Interdisciplinary Journal of Nonlinear Science, 17, 026103
- Erdos, P., & Rényi, A. 1960, Publ. Math. Inst.Hung. Acad. Sci, 5, 17
- Falconer, D., Barghouty, A. F., Khazanov, I., & Moore, R. 2011, Space Weather, 9, n/a, s04003
- Falconer, D. A., Moore, R. L., & Gary, G. A. 2008, The Astrophysical Journal, 689, 1433
- Floyd, R. W. 1962, Commun. ACM, 5, 345
- Fronczak, A., Fronczak, P., & Hołyst, J. A. 2004, Phys. Rev. E, 70, 056110

- Gallagher, P. T., Moon, Y. J., & Wang, H. 2002, Sol. Phys., 209, 171
- Georgoulis, M. K., & Rust, D. M. 2007, The Astrophysical Journal Letters, 661, L109
- Georgoulis, M. K., Tziotziou, K., & Raouafi, N.-E. 2012, The Astrophysical Journal, 759, 1
- Hernndez, I. G., Lindsey, C., Braun, D. C., et al. 2013, Journal of Physics: Conference Series, 440, 012029
- Howard, R. F. 1989, SoPh, 123, 271
- —. 2000, Journal of Astrophysics and Astronomy,21, 119
- Humphries, M., Gurney, K., & Prescott, T. 2005, Proc Biol Sci, doi:10.1098/rspb.2005.3354
- Humphries, M. D., & Gurney, K. 2008, PLOS ONE, 3, 1
- Kim, J., & Wilhelm, T. 2008, Physica A: Statistical Mechanics and its Applications, 387, 2637
- Künzel, H. 1959, Astronomische Nachrichten, 285, 271
- Leka, K. D., & Barnes, G. 2003, The Astrophysical Journal, 595, 1277
- Lindsey, C., & Braun, D. C. 2000, Science, 287, 1799
- Lotfi, N., & Darooneh, A. H. 2012, The European Physical Journal B, 85, 23
- —. 2013, Physica A: Statistical Mechanics and its Applications, 392, 3061
- Mandelbrot, B. B. 1975, Zeitschrift für Wahrscheinlichkeitstheorie und Verwandte Gebiete, 31, 271

- Mason, J. P., & Hoeksema, J. T. 2010, The Astrophysical Journal, 723, 634
- Mei, S., Zhang, X., & Cao, M. 2011, Complex Small-World Power Grids (Berlin, Heidelberg: Springer Berlin Heidelberg), 161–178
- Newman, M. E. 2003, SIAM Rev, 45, doi:10.1137/S003614450342480
- Peng, C.-K., Buldyrev, S. V., Havlin, S., et al. 1994, PhRvE, 49, 1685
- Priest, E., & Forbes, T. 2002, The Astronomy and Astrophysics Review, 10, 313
- Raboonik, A., Safari, H., Alipour, N., & Wheatland, M. S. 2017, The Astrophysical Journal, 834, 11
- Rezaei, S., Darooneh, A. H., Lotfi, N., & Asaadi, N. 2017, Physica A: Statistical Mechanics and its Applications, 471, 80
- Rubinov, M., & Sporns, O. 2010, NeuroImage, 52, 1059, computational Models of the Brain
- Sammis, I., Tang, F., & Zirin, H. 2000, The Astrophysical Journal, 540, 583
- Schrijver, C. J. 2007, The Astrophysical Journal Letters, 655, L117
- Steen, M. v. 2010, Graph theory and complex networks: an introduction (Lexington: Maarten van Steen)

- Stelzl, U., Worm, U., Lalowski, M., et al. 2005,
 Cell, 122, 957
- SunPy Community, T., Mumford, S. J., Christe, S., et al. 2015, Computational Science and Discovery, 8, 014009
- Tang, C., & Bak, P. 1988, Phys. Rev. Lett., 60, 2347
- Telesford, Q. K., Joyce, K. E., Hayasaka, S., Burdette, J. H., & Laurienti, P. J. 2011, Brain Connect., 1, 367
- Wang, F. Y., & Dai, Z. G. 2013, Nat Phys, 9, 465
- Watts, D. J., & Strogatz, S. H. 1998, Nature, 393, 440
- Weron, R. 2002, Physica A: Statistical Mechanics and its Applications, 312, 285
- —. 2011, HURST: MATLAB function to compute the Hurst exponent using R/S Analysis, ,
- Zhang, J., Kundu, M. R., & White, S. M. 2001, SoPh, 198, 347
- Zhang, J., Wang, Y., & Liu, Y. 2010, The Astrophysical Journal, 723, 1006